

A revised relationship between fracture toughness and Y_2O_3 content in modern dental zirconias

Renan Belli ^{1,*}, Katrin Hurlé ^{2,§}, Jana Schürlein ¹, A. Petschelt ¹, Katharina Werbach ³, Herwig Peterlik ³,
Torsten Rabe ⁴, Björn Mieller ⁴, Ulrich Lohbauer ¹

¹ Friedrich-Alexander-Universität Erlangen-Nürnberg (FAU), Zahnklinik 1 – Zahnerhaltung und Parodontologie, Forschungslabor für dentale Biomaterialien, Glueckstraße 11, 91054 Erlangen, Germany

² Friedrich-Alexander-Universität Erlangen-Nürnberg (FAU), GeoZentrum Nordbayern, Mineralogy, Schlossgarten 5a, 91054 Erlangen, Germany

³ Faculty of Physics, University of Vienna, Boltzmannngasse 5, A-1090 Vienna, Austria.

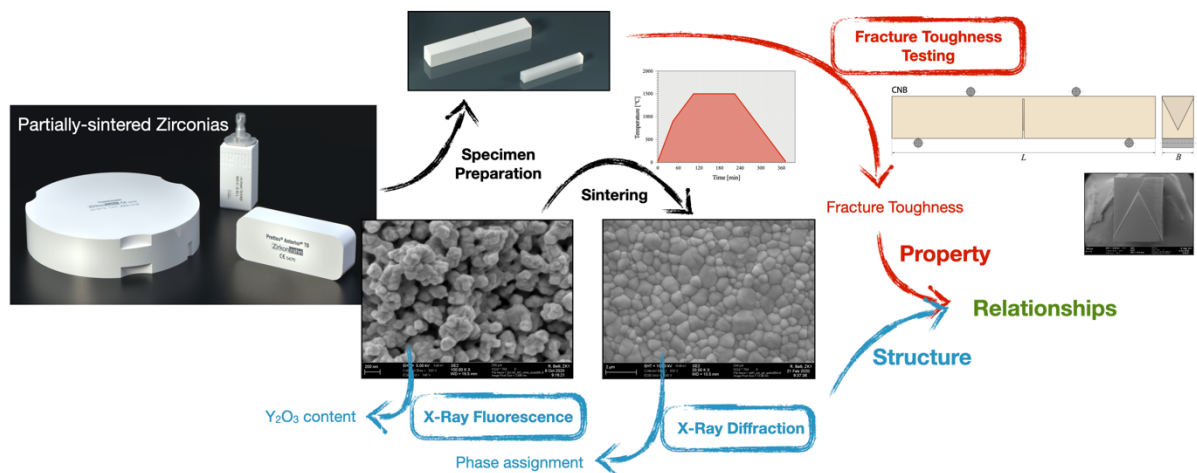
⁴ Bundesanstalt für Materialforschung und -prüfung (BAM), Division Advanced Technical Ceramics, 12200, Berlin, Germany

Original full-length article

Keywords: Dental; Yttria; Zirconia; Fracture toughness; X-Ray-Diffraction; Power-law.

Abstract

The relationship between fracture toughness and Yttria content in modern zirconia ceramics was revised. For that purpose, we evaluated here 10 modern Y_2O_3 -stabilized zirconia (YSZ) materials currently used in biomedical applications, namely prosthetic and implant dentistry. The most relevant range between 2-5 mol% Y_2O_3 was addressed by selecting from conventional opaque 3 mol% YSZ up to more translucent compositions (4-5 mol% YSZs). A technical 2YSZ was used to extend the range of our evaluation. The bulk mol% Y_2O_3 concentration was measured by X-Ray Fluorescence Spectroscopy. Phase quantification by Rietveld refinement are supplied by considering only two tetragonal phases or an additional improbable cubic phase. A first-account of the fracture toughness (K_{Ic}) of the partly-sintered materials is given, which amounted to 0.4 – 0.7 $MPa\sqrt{m}$. In the fully-densified state, an inverse power-law behavior was obtained between K_{Ic} and bulk mol% Y_2O_3 content, whether using only our measurements or including literature data, challenging some established relationships.



* Corresponding author.

Renan Belli (tel.: +49-09131-85-43741, e-mail address: renan.belli@fau.de).

§ These authors contributed equally to this work.

1. Introduction

In an attempt to supply the current high demand for technical guidance, the recent review of Zhang and Lawn [1] in the most prominent dental scientific journal sought to educate readers on the state-of-the-art regarding physical and mechanical properties of commercially available zirconia materials for use as dental prosthetic reconstructions. Though, in a table aimed to enlighten, only ranges of values were given. As it seems, this was not by lapse, rather by lack of alternative. Inadequacies in testing procedures, thought to be systemic in the dental research community, have been heavily addressed recently [2-4], followed by guidelines for improvement [5-8]. Yet, reliable mechanical characterization, especially by means of fracture toughness (K_{Ic}) testing, is still in shortage [6]. More so for new, high-yttria content ‘translucent’ zirconias, despite the explosive trend of prescribing zirconias as monolithic constructs in clinical dentistry [9].

Dental zirconias are mostly delivered as intermediate pre-sintered “white-bodies”, produced by powder compaction and long duration sintering at low-temperatures (900-1000 °C), i.e. bisque firing. At this stage, particles are only partially fused together, density is low and porosity is high, making for easy machinability. The subsequent damage induced by CAM machining must be therefore sustained by the porous white-body as opposed to the approach of hard-machining of fully-densified materials. Not coincidentally, fractographic analysis of retrieved in vivo zirconia fractures have shown fracture origins only compatible to damage having been inflicted to the white-body during machining, before the densification sintering ever took place [10]. The fracture toughness of the white-body is therefore of high importance, as it defines the resistance against crack initiation during machining, too. In the dental literature, one finds no report on the fracture toughness of white-bodies of dental zirconia; in the technical community, this problem has been long recognized.

In this contribution, we attend to these inadvertences.

To bypass the well-known difficulties in fracture toughness testing of zirconia materials [11, 12], we use here a ‘sharp-crack’ testing method to compare polycrystalline ZrO_2 stabilized with xY_2O_3 (being $x = 2 - 5$ mol%) from five important manufacturers, each represented by two different compositions, one being a conventional ‘opaque’ 3YSZ (yttria-stabilized zirconia). Translucent YSZs are doped with 1-2 mol% stabilizer in excess to 3 mol% Y_2O_3 , a strategy used to allegedly foster the growth of large grains of a cubic phase, thereby improving light transmittance [13]. The exchange of tetragonal for more of the supposed cubic allotrope in YSZ compositions is known to be done at the expense of flexural strength, a property strongly related to fracture toughness in ceramic materials. Both properties are used as elective parameters for determining clinical indication in dentistry, as well as for product certification based on requirements established in testing norms (e.g. ISO 6872 [14]). Low K_{Ic} -values are expected for YSZs having less of the metastable tetragonal phase, which is responsible for the mechanism of transformation toughening and the moderately high K_{Ic} of 3YSZ, of approx. $4.5 \text{ MPa}\sqrt{\text{m}}$. Stabilization with 4 – 5 mol% Y_2O_3 should therefore negatively affect K_{Ic} -values, due to the low relative tetragonal content; the clinical indication of prosthetic constructs (e.g. span length, cross-sectional area) of these YSZ materials are consequently limited to fractions of that of 3YSZ. In turn, by reducing the stabilizer content, K_{Ic} -values are expected to increase. The nature of this dependency (i.e. fracture toughness vs. Y_2O_3 content) however, given the shortage of systematic evaluations, summed to testing variability and a somewhat intricate phase characterization, is yet to be resolved. We forgo the use of experimental batches to tackle this issue from the perspective of materials finding real-life applications, with focus on biomedical zirconias.

We hereby ultimately report on the actual bulk Y_2O_3 content of ten commercial dental zirconias ranging from nominal 3 mol% to 5 mol%, and discuss aspects related to phase assignment and quantification using X-Ray diffraction and Rietveld refinement. We extend the range of studied Y_2O_3 content by evaluating a 2YSZ for technical applications, allowing us to provide an apparent power-law relationship between stabilizer content and the fracture toughness of modern zirconia materials having commercial applicability. An account of the fracture toughness of dental zirconias in the partly-sintered state is given first-hand.

2. Materials and Methods

2.1. Materials

The selection of materials to be evaluated in this study was based on the degree of stabilization with Y_2O_3 . For each of the five manufacturers (all leading suppliers of dental zirconia products), two materials were selected, being one of them a conventional (nominal) 3 mol% Y_2O_3 indicated for larger prosthetic reconstructions, and the other a ‘translucent’ variant, i.e. stabilized with (nominal) 4 mol% or 5 mol% Y_2O_3 (as specified by the manufacturer), the latter indicated for reduced prosthetic constructs, e.g. anterior bridges, crown-over-implants, single crowns, onlays and inlays.

Sintering was performed in a bottom-lift oven (Vita Zircomat 6000 M Speed, Vita Zahnfabrik, Germany) that allows flexible programming of the heating and cooling curves. The sintering parameters were maintained strictly according to the manufacturers’ recommendations so to obtain the microstructure that is aimed for during application. The maximum sintering temperature varied therefore from material to material according to the manufacturers’ instructions for use, between 1500 °C and 1600 °C, for a period between 120 and 145 min, with slow cooling taking place inside the oven overnight.

In order to widen the range of stabilizer content tested, we further analyzed a nominal 2 mol% Y_2O_3 stabilized zirconia material from a nanopowder produced by emulsion detonation synthesis (Innovnano SA, Portugal). The powder as-received was pressed uniaxially at 60 MPa, with subsequent isostatic pressing at 200 MPa, and sintered for 4 hours at 1375 °C.

The commercial brand names, their manufacturers, LOT numbers, together with the specified Y_2O_3 mol% as given by the manufacturers, are listed in Table 1. Important to note that all analyses and tests were conducted within one batch.

Table 1. Commercial materials analyzed in this study, their specified stabilizer content, manufacturers, batches, peak temperature and dwell time.

Material	Specified Y_2O_3 [mol%]	Manufacturer	Batch (Lot Nr.)	Peak temperature [°C] / Dwell time [min]
IPS e.max [®] ZirCAD MO	3	Ivoclar-Vivadent AG, Liechtenstein	V38361	1500 / 120
IPS e.max [®] ZirCAD MT	4		W12059	1500 / 120
Lava [™] Plus	3	3M Deutschland GmbH, Germany	3343987	1500 / 120
Lava [™] Esthetic	5		3515130	1500 / 120
Cercon [®] ht	3	Dentsply-Sirona Inc., Germany	18029331	1520 / 145
Cercon [®] xt	5		18031834	1520 / 145
Katana [™] ML	4	Kuraray Noritake Dental Inc., Japan	DTHYP	1500 / 120
Katana [™] STML	5		DLEEQ	1550 / 120
Prettau [®]	3	Zirkonzahn GmbH, Italy	ZB3235E	1600 / 120

Prettau® Anterior	5		ZB8068A	1500 / 120
Innovnano 2YSZ	2	Innovnano SA, Portugal	1801PA801	1350 / 240

2.2. Structural Characterization

2.2.1. Determination of Y_2O_3 content by X-Ray Fluorescence (XRF) Spectroscopy

Dental zirconia products with different degrees of translucency are commonly labeled by manufacturers to fall within one of three categories “3mol%”, “4mol%”, or “5mol%” stabilization with Y_2O_3 , for which only a range is given in weight% in the respective composition datasheets. In order to determine the actual amount of Y_2O_3 and Al_2O_3 in the commercial materials, XRF spectroscopy was conducted on pulverized pre-sintered samples by an accredited laboratory (Terrachem GmbH, Mannheim, Germany) following DIN 51001:2003-08. The amount of Y_2O_3 and Al_2O_3 in mol% (error < 0.15 mol%) was calculated from the wt.% provided by XRF analysis and the molar masses of the corresponding oxides.

2.2.2. Quantitative XRD analysis

The quantitative phase composition of the commercial YSZ ceramics was determined by X-ray diffraction (XRD). The ceramics were measured in their bulk form (plates) and fixed into special sample holders using plasticine. Two separate plates of each product were analyzed.

Measurements were performed at a D8 diffractometer (Bruker AXS, Karlsruhe) equipped with a 9-fold sample changer. The following parameters were applied: Range 25° - 90° 2θ ; step size 0.011° 2θ ; integration time 1 s; radiation: copper $K\alpha$; generator settings: 40 kV, 40 mA; divergence slit: 0.3° ; detector: LynxEye.

Quantitative evaluation of the diffraction patterns was performed by Rietveld refinement using the software TOPAS V5 (Bruker AXS, Karlsruhe, Germany). It was reasonably assumed that the samples were 100 % crystalline. The structure models for the refinement of the crystalline $ZrO_2(Y)$ phases were obtained from the ICSD database (FIZ Karlsruhe, Germany) (Table 1). Since for some samples not all reflections could be covered by one cubic and one tetragonal structure and the monoclinic phase was clearly absent, the structure for tetragonal $ZrO_2(Y)$ was inserted twice and refined with different lattice parameters. Refined parameters were scale factor, lattice parameters, crystallite size, and microstrain. For the monoclinic phase, additionally a preferred orientation was inserted for both (1 -1 -1) and (0 0 1) reflections. A Chebychev polynomial of 3rd order was used for the background.

Table 2. ICSD structures used for refinement of the different ZrO_2 modifications.

Phase	ICSD #	Space group	Authors
$ZrO_2(Y)$	417639	Monoclinic $P2_1/c$	Jovalekic et al. [15]
$ZrO_2(Y)$	89428	Tetragonal $P4_2/nmc$	Wang et al. [16]
$ZrO_2(Y)$	89429	Cubic $Fm-3m$	Wang et al. [16]

2.2.3. Calculation of Y_2O_3 content in tetragonal and cubic $ZrO_2(Y)$ from lattice parameters

The Y_2O_3 content of the tetragonal $ZrO_2(Y)$ phases was estimated from the lattice parameters obtained by Rietveld refinement using the equation presented by Miller et al. [17], which is based on a diagram presented by Scott [18]. In this approach, the $YO_{1.5}$ content [mol%] is derived from the tetragonality c/a of the phase according to:

$$YO_{1.5}[\text{mol}\%] = \frac{1.0223 - \frac{c}{a_t}}{0.001319}, \quad (1)$$

where $a_t = \sqrt{2}a$. The content of Y_2O_3 in mol% can then be obtained by the conversion:

$$Y_2O_3[\text{mol}\%] = \frac{YO_{1.5}[\text{mol}\%]/100}{2 - YO_{1.5}[\text{mol}\%]/100} \cdot 100. \quad (2)$$

This method is more reliable than the determination of the $YO_{1.5}$ content directly from the lattice parameters, as suggested by Toraya [19], since possible device specific effects can be eliminated by using the ratio of the lattice parameters (tetragonality).

The Y_2O_3 content of the cubic modification $Y_2O_{3(\text{cubic})}$ [mol%] was additionally estimated from the Rietveld wt.% quantities of the different ZrO_2 modifications, the Y_2O_3 content of the tetragonal $ZrO_2(Y)$ phases calculated from tetragonality ($Y_2O_{3(t)}$ [mol%] for the Y-lean, and $Y_2O_{3(t')}$ [mol%] for the Y-rich modification), together with the Y_2O_3 content of the bulk sample $Y_2O_{3(\text{bulk})}$ [mol%], determined by XRF. For this purpose, Eq. (3) was applied:

$$Y_2O_{3(\text{cubic})}[\text{mol}\%] = \frac{Y_2O_{3(\text{bulk})}[\text{mol}\%] - \frac{\text{wt.}\%(t) \cdot Y_2O_{3(t)}[\text{mol}\%]}{100} - \frac{\text{wt.}\%(t') \cdot Y_2O_{3(t')}[\text{mol}\%]}{100}}{\text{wt.}\%(\text{cubic})} \cdot 100 \quad (3)$$

For morphological characterization, sintered samples were lapped using 9 μm to 1 μm Al_2O_3 particle suspensions, thermally etched at 1300 $^\circ\text{C}$ for 1 h, sputter-coated with gold and observed in a field-emission scanning electron microscope (Auriga, Zeiss).

2.3. Mechanical Characterization

2.3.1 Determination of Elastic Constants

The density ρ was determined geometrically, the Young's modulus E , and the Poisson's ratio ν , of the partially-sintered and densely sintered samples were measured using Resonant Ultrasound Spectroscopy (RUS) as described in a previous study [20].

2.3.2. Fracture toughness (K_{Ic}) measurement of partially-sintered and sintered samples

For the measurement of the fracture toughness using the Chevron Notched Beam (CNB) method, round blanks of partially-sintered material were used as received from the manufacturers in order to allow the production of beams of 45 mm in length (L), as well as short beams with $L = 25$ mm, except for IPS e.max[®] CAD MO, for which only B 40 L blocks were used (allowing only short beams to be produced). Long beams having dimensions *Length* x *Height* x *Width* (L x W x B) of 45 x 6.35 x 6.35 mm³, corresponding to 'Configuration B' in ASTM C 1421 [21], were employed to determine the fracture toughness of the partially-sintered (white-body) materials, to be tested in three-point bending with a span of 40 mm. For the measurement of the fracture toughness of the materials after densification sintering, the 'Configuration A' according to ASTM C 1421, having a cross section W x $B = 4$ x 3 mm² (a geometry also standardized in ISO 24370 [22] and EN 14425-3 [23]) was used, having $L = 25$ mm to be measured in four-point bending with outer and inner spans of 20 mm and 10 mm, respectively, as allowed in the aforementioned standards. For the material IPS e.max[®] ZirCAD MO only Configuration A was used for either the white-body and for the sintered material. Beams were sawed from the partially-sintered blanks/block under water

lubrication using an automatic cutting saw (Bühler 5000) and a diamond-coated copper disc. Beams for Configuration B meant to be sintered later, were cut in oversized dimensions to account for ~20 % linear shrinkage. Figure 1 illustrates both geometries used. The notch at the midspan of the beams as intended for the CNB method, following the notch dimensional ratios recommended in the aforementioned standards, was produced in all specimens at the white-body stage (prior to sintering), by means of successive cuts using a rotating 0.15 mm-thick diamond disc. Up to twelve specimens were produced per material for each experimental group accounting for the eventuality of invalid tests.

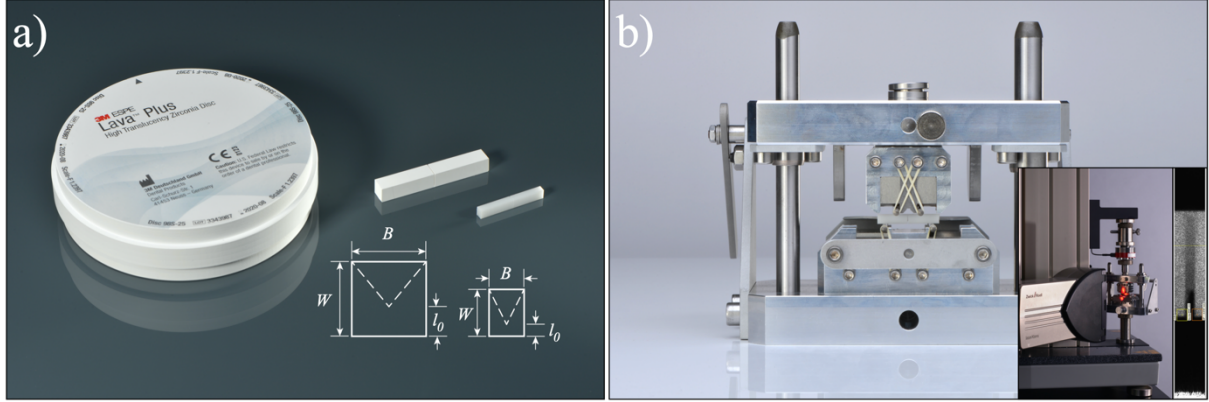


Fig. 1. (a) Pre-sintered dental zirconia blank, from which two beam geometries for the CNB specimens were produced: 6.35 x 6.35 mm² and 4 x 3 mm² cross-sections, for the pre-sintered and sintered specimens, respectively. (b) Fully-articulated jig used for testing in 4-point bending, coupled with a laser-unit for speckle image correlation to track the specimen deflection and the presence of subcritical crack growth before fracture.

Notched specimens were sintered with the notch tip directed upwards, with all specimens per group sintered together in the same cycle. After sintering, the specimens were checked for bending deformations, which when present, were made plane-parallel in a grinding machine under water irrigation (only minimal deformations were allowed). Afterwards, the notch dimensions on the lateral sides of the specimens were measured under a stereomicroscope coupled with a digital camera and accompanying software. Before testing, the specimens were dried in an oven at 150 °C together with a silicon oil bath, into which the specimens were immersed after 3 hours of drying. This was meant to protect the crack that pops at the tip of the triangular notch during testing from environmental water, which could induce stress corrosion crack growth and influence the obtained K_{Ic} -values [24]. Specimens coated with silicon oil were tested at a loading rate of 0.005 mm/s (in order to induce a pop-in crack) in a custom testing jig [6], with load-line displacement controlled by an imaging system (LaserXtens, Zwick/Roell, Germany) based on the image digital correlation approach for accurate detection of the stable crack growth at the tip of the notch before instability. The K_{Ic} was then calculated from the maximum force at fracture F_{max} [21]:

$$K_{Ic} = \frac{F_{max}(S_o - S_i)}{BW^{3/2}} \cdot \frac{Y_{max}^*}{\sqrt{10^3}} \quad (4a)$$

being S_o the outer span length and S_i the inner span length, and:

$$Y_{max,3PB}^* = \frac{0.760 - 3.6364(l_0/W) + 3.1164(l_1/W) - 1.2782(l_1/W)^2 + 0.3609(l_1/W)^3}{1 - 3.1199(l_0/W) + 3.0558(l_0/W)^2 - 1.0390(l_0/W)^3 + 0.0608(l_1/W)} \quad (4b)$$

for the 3-point bending set-up using configuration B, for which S_i in Eq. 1 is equal 0, and for four-point bending with the configuration A:

$$Y_{\max,4PB}^* = \frac{0.3874 - 3.0919(l_0/W) + 4.2017(l_1/W) - 2.3127(l_1/W)^2 + 0.6379(l_1/W)^3}{1 - 2.9686(l_0/W) + 3.5056(l_0/W)^2 - 2.1374(l_0/W)^3 + 0.0130(l_1/W)} \quad (4c)$$

where l_0 is the distance between the bottom edge of the beam and the tip of the Chevron notch, and l_1 an arithmetic mean of the unnotched segments on the sides of the beam. The ratios l_0/W and l_1/W were kept within the ranges $0.175 < l_0/W < 0.225$ and $0.95 < l_1/W < 1$ for configuration A and $0.382 < l_0/W < 0.420$ and $0.95 < l_1/W < 1$ for configuration B, in order to minimize the error to a maximum of 1 %. The l_0 was measured after fracture in a stereomicroscope coupled with a digital camera and accompanying software. Specimens showing load-deformation curves diverging from those depicted in the aforementioned standards (absence of stable crack propagation before instability) were regarded as invalid tests and not included in the analysis. The aforementioned standards define a sample number of 5 valid specimens as sufficient for evaluation. We made sure to obtain 5 valid specimens for the partially-sintered state, and 9 to 10 specimens for the sintered materials.

Our CNB testing procedures have been recently validated using a Standard Reference Material (see Ref.[25]).

3. Results and Discussion

3.1. The white-bodies

SEM images of the microstructure, obtained from fracture surfaces, reveal sharp-edged particles of <100 nm in size, passed from the stage of neck-formation (see Fig. 2a), creating a concave open porosity network.

The density is about half, the Poisson's ratio approx. two-thirds, and the Young's modulus about one-tenth of the sintered materials, the latter corresponding roughly to the ratio of fracture toughness in white-bodies to sintered samples (see Table 3). Although there is no obvious relation between Young's modulus, Poisson's ratio, density and fracture toughness within the same white-body material, it should be noticed that the two samples with the highest Young's modulus also exhibited the highest fracture toughness.

Table 3. Elastic properties (E , ν), density (ρ) and fracture toughness (K_{Ic}) of the white-bodies.

Material	E [GPa]	ν	ρ [g/cm ³]	K_{Ic} [MPa√m]
IPS e.max [®] ZirCAD MO	20.81 ± 0.32	0.322 ± 0.020	3.060 ± 0.130	0.43 ± 0.03
Lava [™] Plus	14.78 ± 0.23	0.192 ± 0.020	3.195 ± 0.016	0.53 ± 0.02
Cercon [®] ht	15.37 ± 0.24	0.188 ± 0.020	3.196 ± 0.013	0.48 ± 0.01
Prettau [®]	12.72 ± 0.20	0.158 ± 0.020	3.131 ± 0.013	0.56 ± 0.02
Katana [™] ML	29.40 ± 0.45	0.291 ± 0.020	3.060 ± 0.098	0.63 ± 0.07
IPS e.max [®] ZirCAD MT	18.62 ± 0.28	0.183 ± 0.020	3.222 ± 0.021	0.55 ± 0.02
Katana [™] STML	31.34 ± 0.47	0.208 ± 0.020	3.116 ± 0.007	0.71 ± 0.02
Lava [™] Esthetic	17.70 ± 0.27	0.196 ± 0.020	3.197 ± 0.015	0.59 ± 0.02
Cercon [®] xt	15.83 ± 0.24	0.139 ± 0.020	3.221 ± 0.013	0.44 ± 0.03
Prettau [®] Anterior	15.63 ± 0.24	0.292 ± 0.020	3.125 ± 0.010	0.38 ± 0.06

Apart from the fact that zirconia white-bodies are porous materials and naturally weaker than dense solids, they are subjected to machining challenges much like those employed for their fully-dense glass-ceramic counterparts.

For the latter materials, the damage introduced during machining in dental CAM systems seems to attract attention in scales commensurate to its practical significance, specifically due to their lower fracture toughness. Exemplarily, defects caused by diamond grinding in feldspathic ceramics ($K_{Ic} \sim 1.2 \text{ MPa}\sqrt{\text{m}}$) have shown to lead to up to 56% strength deterioration [26]. For lithium (di)silicates machined in their partially-crystallized state ($K_{Ic} \sim 0.9 - 1.2 \text{ MPa}\sqrt{\text{m}}$ [27]), rough grinding with diamond burs was shown to induce subsurface cracks up to $18 \mu\text{m}$ in depth [27]. Those cracks heal during the second crystallization firing by viscous flow and capillarity forces [27, 28], as the residual glass is heated above its glass transition temperature. This is not the case for zirconia. Qualitative evidence shows that cracks created in the white-bodies of dental zirconias do not heal during final sintering [6, 29], as viscous flow is not taking place at those temperatures. Even though the cutting tools for zirconia white-body machining are generally not diamond-based, the local stresses inflicted to the white-bodies during machining are certainly not insignificant; added to a low K_{Ic} -value, a scenario that predisposes crack initiation is probable.

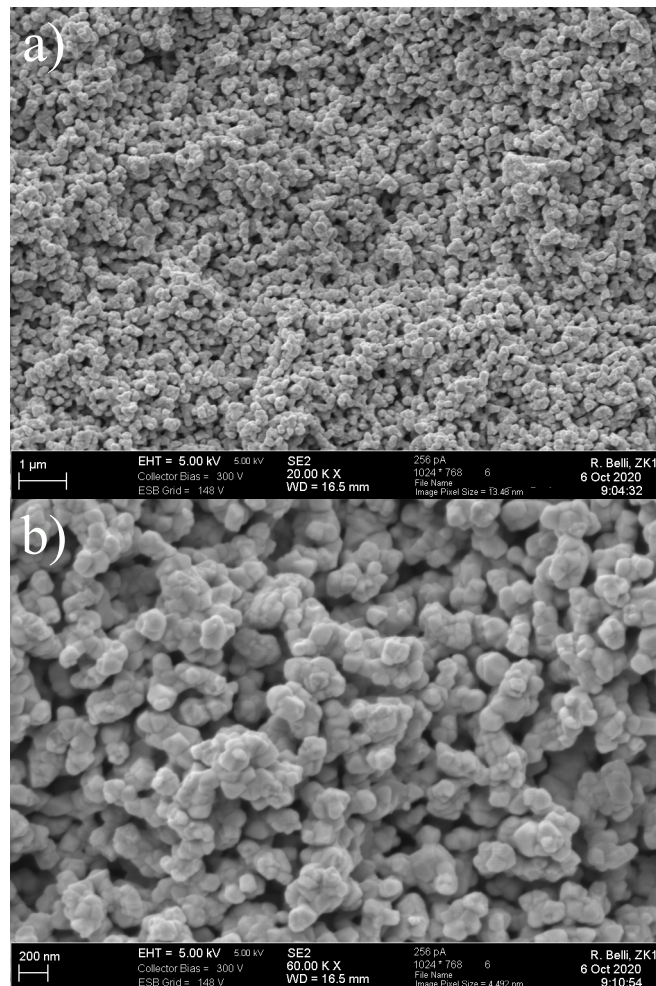


Fig. 2. Example of the microstructure of a partly-sintered white-body, showing partially fused particles and an open concave porosity.

No significant differences related to the stabilizer concentration, concerning the K_{Ic} of the white-bodies, could be established. In other words, it seems that the microstructure and properties of this frozen-in state – the white-body – has no bearing on the development of the fracture toughness after full densification. Notwithstanding, differences

among commercial materials reached up to ~90%, with higher values for the Katana materials. This is probably linked to the individual processing factors undertaken by the different manufacturers, especially sintering parameters, i.e. temperature and time, since other factors related to powder processing, such as binder type and fraction, and size distribution of primary and secondary particles (agglomerates) are defined by the powder supplier. The majority of dental zirconia manufacturers are supplied by Tosoh Corp., which provide powders composed of 40 nm primary particles (which match the microstructural units seen in Fig. 2b) mixed with 3 wt.% binders, resulting in a unimodal particle size distribution of spherical powder aggregates of 20 – 200 μm in size ($d_{50} \sim 50 \mu\text{m}$, [30]), e.g. in their 3 mol.% Y_2O_3 powder TZ3YBE. The pressing is usually made in-house by the manufacturers or outsourced, prior to the bisque firing, during which the binder is also removed. The comparable values for density among the pre-sintered materials, together with their microstructural similarity, seem to suggest that all materials present similar degrees of densification, that is, the pre-sintering was interrupted at equivalent stages. Research in optimizing those steps, aimed at achieving white-bodies that are more resistant to machining damage, are generally lacking. The increase in densification of white-bodies should contribute to that objective, with the trade-off involving machining tool wear and overall machining time, and the risk of increased brittleness.

3.2. Fully-densified Materials

3.2.1. Composition and microstructure

The measured $x\text{Y}_2\text{O}_3$ concentration of the dental commercial materials listed in Table 1 by XRF is given in Tables 4 and 5. Compared to the values stated by the manufacturers, the actual $x\text{Y}_2\text{O}_3$ concentrations in the samples are, in general, slightly higher. For the advertised 3YSZ materials the deviation is less significant, with Y_2O_3 fractions being underreported by up to 0.4 mol% in the 5YSZ materials. The 2YSZ material turned out to contain 1.89 mol% Y_2O_3 (see Table 6). Because some materials showed very similar Y_2O_3 content, we will in the text hereafter refer only to compositions having significantly different amounts of stabilizer, as in $x = 1.9, 3.1, 4.1, 4.3, 4.8$ and 5.4 . In Fig. 3 the microstructural appearance of the most relevant materials is shown, with labels referring to their mol% Y_2O_3 fraction as measured by XRF (assignment to the corresponding materials can be made by means of Tables 4 to 6).

Fig. 3a shows the microstructure of 1.9 mol% Y_2O_3 material. It represents the fine-grained microstructure typical for technical, strength optimized 2YSZ and 3YSZ materials. The grain size is between 200 nm and 500 nm. Fig. 3b shows a 1. Generation dental 3YSZ (3.05 mol%) with 0.3 mol% Al_2O_3 . Here, the grain size is visibly larger compared to Fig 3a, indicating an oversintering of the material if compared to the microstructure of typical technical 3YSZs. Fig. 3c exemplarily shows a 2. Generation 3YSZ with reduced Al_2O_3 content. This and the following microstructures result from Al_2O_3 reduction and Y_2O_3 increase by the manufacturers to increase translucency at the expense of strength (2. to 4. Generation zirconia). In fact, apart from the materials in Fig. 3a and b, all materials showed very similar microstructures, having an apparent bimodal grain size distribution composed of sparse large grains of well-defined boundaries and smooth surfaces embedded in a corrugated irregular-shaped fine-structure with features of about 50-100 nm in size. These fine grains appear to form groups delimited by a continuous boundary, as if formerly belonging to a single large-sized grain. Some of the large grains showed eventual signs of surface roughening, with regions in the grain having similar microstructural aspects to the fine grains, in a gradual transition (see pointers in Fig. 3f, g and h). The materials in Fig. 3d and 3e could be distinguished visually by having the large grains in smaller and more homogeneous size distribution.

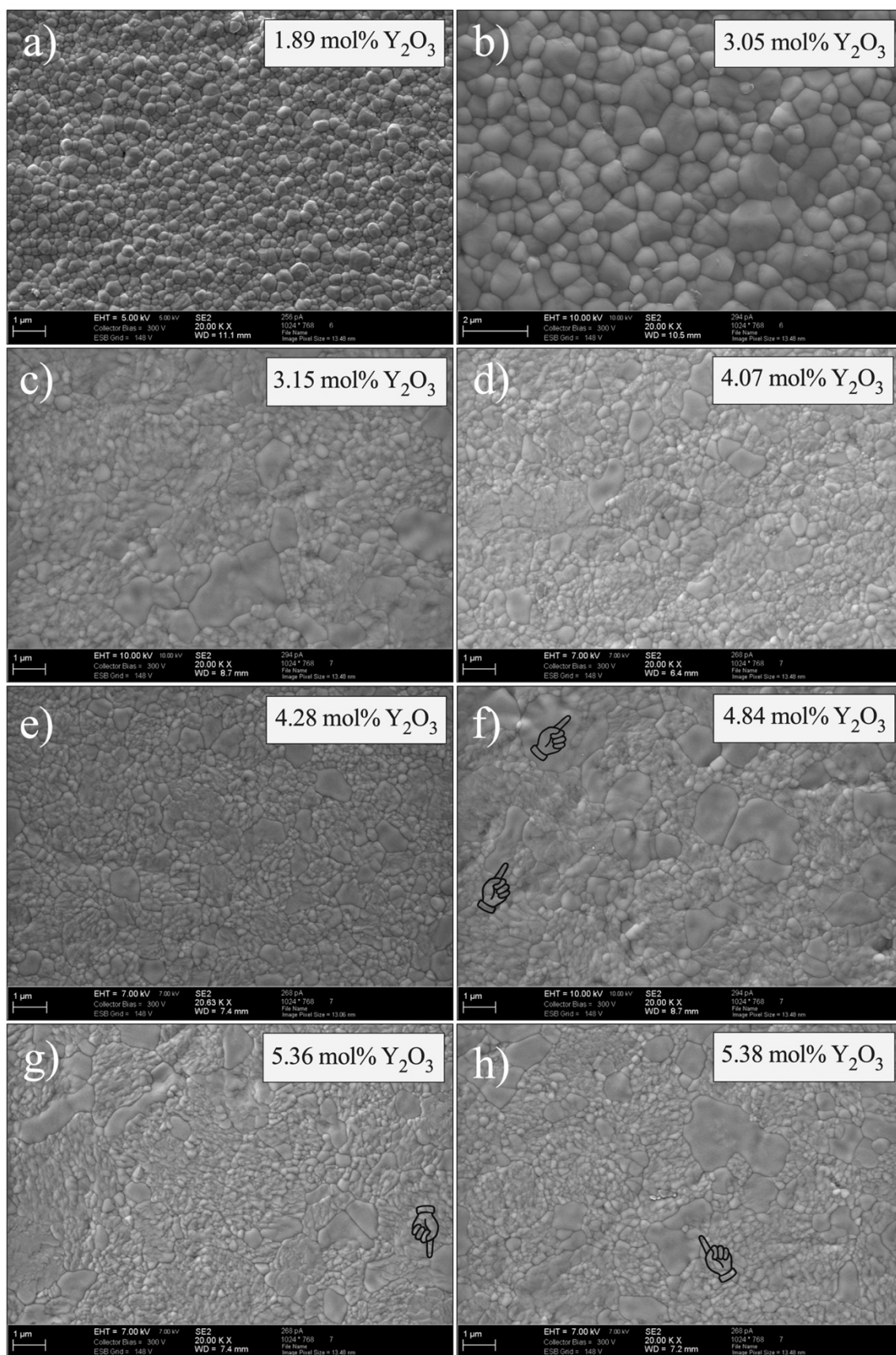


Fig. 3. Microstructure of the surface of the sintered samples as observed in a SEM. Pointers indicate large grains showing a gradient roughening in morphology.

3.2.2. Phase quantification

A screening of the dental literature reveals a pattern of labeling zirconia compositions doped with Y_2O_3 in concentrations 4 – 5 mol% as partially cubic, with fractions ranging from 20 wt% up to 70 wt% [31-34]. The material Katana STML, for instance, has been reported to be composed of 59.9 wt% or 70 wt.% of cubic phase by Ref. [31] and Ref. [33], respectively, as measured by XRD. More often than not, the bulk Y_2O_3 content is estimated solely from the phase quantification, with rare efforts of elemental verification. The alleged cubic phase is accredited the higher translucency in these compositions, due to the isotropic symmetry that reduces light birefringence and grain boundary scattering [13]. These and other studies rely mostly on room-temperature XRD characterization, which has been shown to suffer from several shortcomings, which lead inevitably to misleading phase assignment. Fundamentally, the presence of a cubic phase at room-temperature for compositions < 8 mol% Y_2O_3 is inconsistent with the thermodynamic understanding of phase transitions as illustrated by currently accepted equilibrium phase diagrams of the $\text{ZrO}_2 - \text{Y}_2\text{O}_3$ system [35, 36] (see Fig. 4).

At the sintering temperatures recommended by the manufacturers, only the material having $x = 1.9$ ($x = \text{mol}\% \text{Y}_2\text{O}_3$) is located entirely in the tetragonal field (t), with the four materials having $x = 3.1$ and the two materials having $x = 4.1$ and 4.3 being placed within the metastable extension of the tetragonal field (t'), and all other materials above the $T_0(c/t)$ line within the supersaturated metastable cubic field (c'), as illustrated by the data-points at the sintering temperature in Fig. 4. If the symmetry of the supersaturated t' and c' parent phases at the sintering temperature were to be kept upon cooling, the original t' -phase would persist at room temperature, while the high-temperature c' -phase would undergo a diffusionless, non-suppressible transformation to a tetragonal symmetry down through the $T_0(c/t)$ line [18, 37]. The morphology of the resulting tetragonal domains seems to be predicated on the extent of the available driving force for transformation [38]; if high enough, a twinned morphology ensues from a *displacive/shear* mechanism giving rise to t' [39] (the phase presenting ferroelastic domain switching as toughening mechanism [40]), otherwise a “mottled” structure of highly disordered nanograins arrays [38, 41, 42] where two tetragonal variants coexist: t plus a new, so-called t'' -phase [43]. This t'' phase is transformed from a parent c' -phase by an *ordering* mechanism of the anion sublattice [38], retaining the stabilizer enrichment and attaining a very low tetragonality ($c/a \rightarrow 1$). The t'' -phase is non-transformable to the m -allotrope upon mechanical stress (transformation toughening), in contrast to the t -phase.

Due to the temperature-dependent [44] Y^{3+} segregation, the stability of the parent t' and c' phases during sintering becomes frail, and these two phases have been shown to decompose (de-stabilize) into coherent Y-lean (Y_2O_3 depleted) and Y-rich (Y_2O_3 enriched) phases toward the equilibrium phases t and c very rapidly [41, 42, 45]. After decomposition, t' reflections will remain resolvable in the XRD profile, and fitting will profit from the inclusion of a t' phase on top of the $t + t''$ patterns [46]. The XRD signal of a t' phase, however, is suggested to consist of an artifact resulting from the interfacial coherency strains between the other two tetragonal phases, which gives rise to average lattice parameters [42, 46]. The coexistence of a residual parent t' -phase with other two tetragonal phases is further regarded as incompatible with the accepted theory of nucleation and growth, and thermodynamically inconsistent [45]. The low sensitivity of XRD to perturbations on the anion sub-lattice (from where the tetragonality stems), contributes further to inadequate interpretation of phase evolution, by exhibiting cubic-like peaks in < 15 mol% Y_2O_3 compositions [41, 45-47]. Electron diffraction of TEM samples negates any

cubic structure by revealing forbidden $\{112\}$ -type reflections along the $\langle 111 \rangle$ zone axis [41, 47]. Any c -phase resolved from XRD should therefore be interpreted as t'' in the nanometric mottled microstructure.

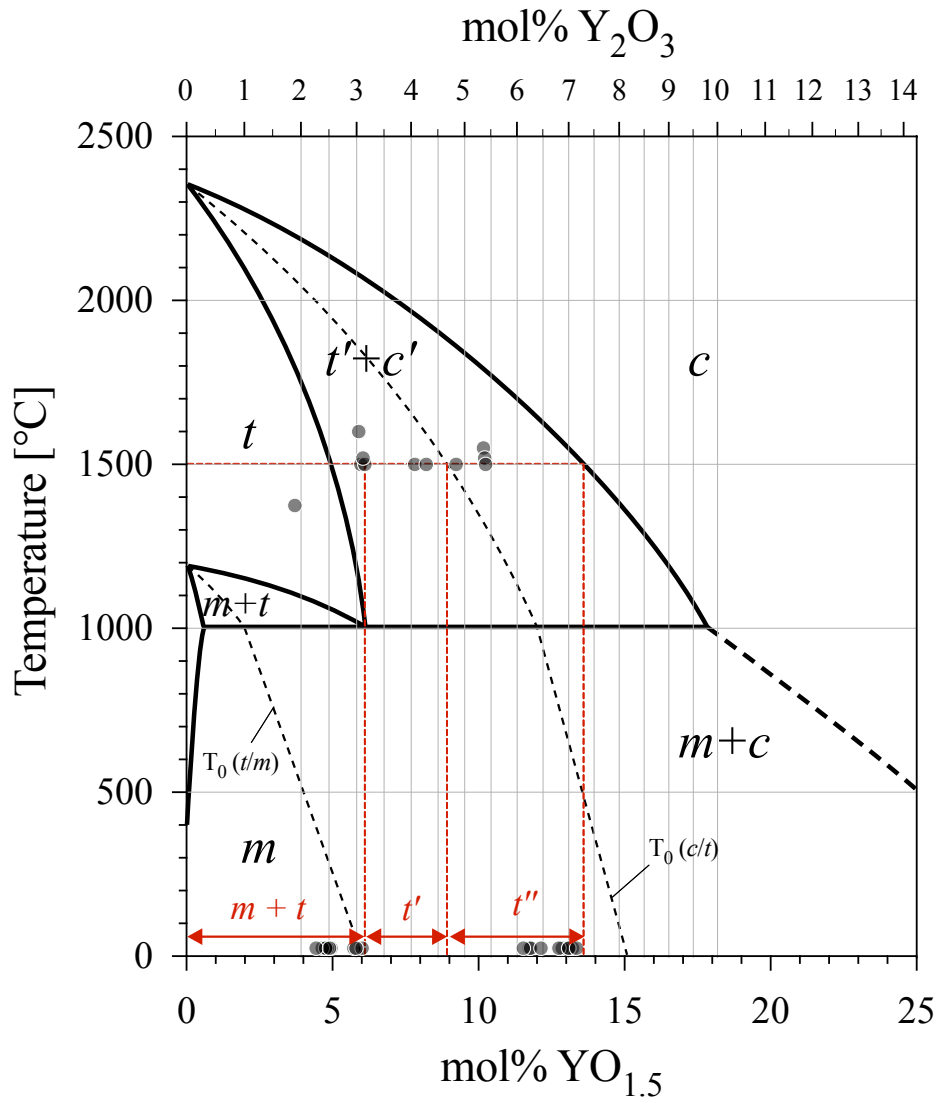


Fig. 4. Phase equilibrium diagram of the $\text{ZrO}_2\text{-Y}_2\text{O}_3$ system after Refs. [35, 36], showing the location of the tested materials at the sintering temperature and after cooling to room temperature according to the Y_2O_3 content in the respective phases. In red, the phases that are found after cooling from sintering temperature.

The phase quantification of the dental zirconia materials was therefore performed here using two different refinement approaches. The first approach considered the presence of three phases: two tetragonal (one Y-lean referred as t -phase, and one Y-rich, referred as t'' -phase) and one cubic ($t + t'' + c$); or considering only the presence of the two tetragonal phases ($t + t''$). Although the approach using only two tetragonal phases is more plausible in view of the phase diagram and the abovementioned TEM evidence, the refinement additionally containing the cubic phase was included for the evaluation and discussion, as addition of the cubic $\text{ZrO}_2(\text{Y})$ structure slightly improved the fit in the Rietveld refinement. The t -phase is the tetragonal phase at room temperature resulting from sintering at temperatures within the t -field and cooled through the $T_0(t/m)$ line (from a direct path for Innovnano,

but from a t -by-product of the $t' \rightarrow t + c'$ decomposition for the materials having $x = 3.1, 4.1$ and 4.3). The t'' -phase is the tetragonal form present at room temperature for samples sintered at temperatures within the metastable extension of the cubic phase and cooled through the $T_0(c/t)$ line.

In Fig. 6 the fitting procedures are illustrated comparing the two approaches. The phase fraction in vol.% calculated by the two refinement approaches is given in Tables 4 and 5, along with lattice parameters and the mol% Y_2O_3 content in the respective phases calculated from Eqs. (1), (2) and (3). By not considering the existence of a cubic phase, the amount of t -phase decreases for the $x = 3.1$ materials, and increases for the $x > 3.1$ materials, due to the redistribution between t and t'' . The relationship between t -phase content and xY_2O_3 is shown in Fig. 6, indicating a better agreement to the $t + t''$ refinement approach (including the extrapolation toward zero t -phase coinciding with 8 mol% Y_2O_3 in the phase diagram), and an overproportionate high amount of t -phase for the $x = 3.1$ materials. This further supports our assumption that the Rietveld refinement including only the two tetragonal phases is actually the correct one. The slight improvement of the Rietveld fit observed by insertion of the cubic phase is no contradiction to this statement, since insertion of more parameters generally can result in better fitting. As the cubic $ZrO_2(Y)$ does not have any unambiguous reflections which are not overlaid by the reflections of the tetragonal phases (see Figure 5c), it is practically impossible to clearly prove or refute the additional presence of cubic $ZrO_2(Y)$ from Rietveld refinement alone.

The tetragonality c/a_t (with $a_t = \sqrt{2}a$) of the t and t'' phases did not change significantly regardless of refinement approach (from 1.014 to 1.016 with decreasing stabilizer content for the t -phase; and from 1.005 to 1.006 with decreasing stabilizer content for the t'' -phase). By considering the existence of only two tetragonal phases, the materials having $x = 5.4$ decomposed toward phases containing the highest Y_2O_3 concentrations (~ 3 mol% in t , and ~ 7.1 mol% in t''), with a trend of lower Y_2O_3 fractions for decreasing x (see room-temperature data-point in the phase diagram in Fig. 3). In the $t + t'' + c$ refinement approach, this relationship is not evident. Furthermore, in this approach the Y_2O_3 content in the cubic phase is always in the range between 4.1 and 5.7 mol.%, which is clearly too low to conform with the expected values from the phase diagram.

In Table 6 the data for the $x = 1.9$ material is given separately for a sample before (surface) and after grinding (interior, see Fig. 5d). No Y_2O_3 content can be presented for the monoclinic modification due to the lack of a suitable formula in the literature.

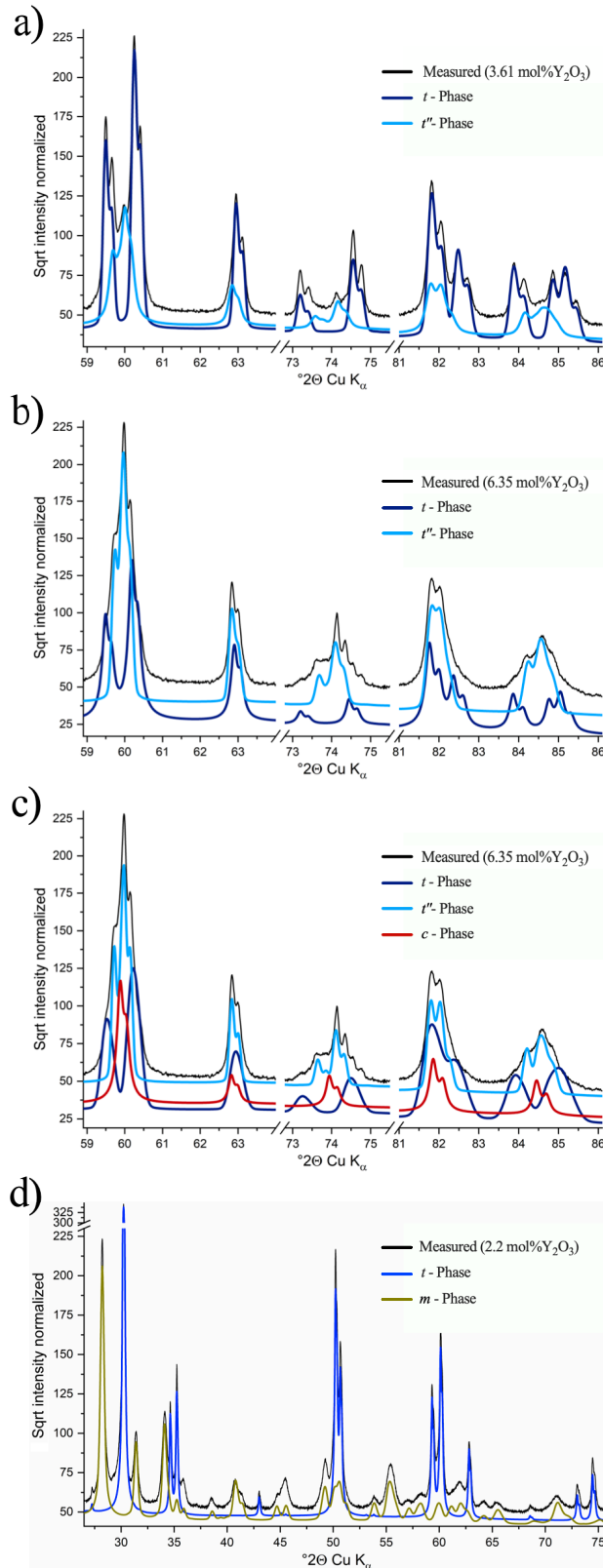


Fig. 5. Diffraction patterns of commercial $\text{ZrO}_2(\text{Y})$ dental ceramics, including the patterns of the different $\text{ZrO}_2(\text{Y})$ modifications refined with software TOPAS V5 (Bruker AXS, Karlsruhe, Germany) using the structures presented in Table 1: a) Cercon[®] ht (representative of samples with lower Y content) refined with two tetragonal structures; b) Cercon[®] xt (representative of samples with higher Y content) refined with two tetragonal structures or c) with two tetragonal and an additional cubic structure. (d) Innovnano 2YSZ material.

Table 4. Bulk Y_2O_3 / Al_2O_3 content (XRF), phase vol.% content (Rietveld), lattice parameters and Y_2O_3 content in each phase (determined from equations (1), (2) and (3)), according to a refinement considering the existence of two tetragonal and one cubic phase ($t + t'' + c$). Values represent the means and standard deviations of two separate samples.

Material	Bulk mol% Y_2O_3 / Al_2O_3 (XRF)	cubic			t (Y-lean)				t'' (Y-rich)			
		vol.%	a [Å]	mol% Y_2O_3	vol.%	a [Å]	c [Å]	mol% Y_2O_3	vol.%	a [Å]	c [Å]	mol% Y_2O_3
IPS e.max® ZirCAD MO	3.08 / 0.300	20.9 ± 0.5	5.1310 ± 0.0001	5.44 ± 0.07	79.1 ± 0.5	3.6045 ± 0.0001	5.1790 ± 0.0001	2.45 ± 0.01	-	-	-	-
Lava™ Plus	3.15 / 0.111	21.2 ± 0.7	5.1312 ± 0.0001	5.37 ± 0.07	78.8 ± 0.7	3.6051 ± 0.0001	5.1786 ± 0.0001	2.55 ± 0.01	-	-	-	-
Cercon® ht	3.12 / 0.049	18.1 ± 0.5	5.1321 ± 0.0001	5.74 ± 0.05	81.9 ± 0.5	3.6053 ± 0.0001	5.1791 ± 0.0001	2.53 ± 0.01	-	-	-	-
Prettau®	3.04 / 0.000	16.5 ± 0.1	5.1325 ± 0.0002	5.53 ± 0.03	83.5 ± 0.1	3.6055 ± 0.0001	5.1793 ± 0.0001	2.54 ± 0.01	-	-	-	-
Katana™ ML	4.07 / 0.112	23.8 ± 0.1	5.1316 ± 0.0001	4.07 ± 0.04	48.5 ± 0.3	3.6039 ± 0.0001	5.1798 ± 0.0003	2.33 ± 0.02	27.7 ± 0.3	3.6227 ± 0.0001	5.1524 ± 0.0003	6.73 ± 0.02
IPS e.max® ZirCAD MT	4.28 / 0.050	23.1 ± 2	5.1347 ± 0.0004	4.50 ± 0.09	46.0 ± 2	3.6056 ± 0.0002	5.1787 ± 0.0001	2.60 ± 0.02	30.5 ± 0.1	3.6230 ± 0.0001	5.1534 ± 0.0001	6.67 ± 0.02
Katana™ STML	5.36 / 0.000	26.9 ± 2	5.1348 ± 0.0001	4.7 ± 0.1	24.2 ± 0.1	3.6094 ± 0.0007	5.1790 ± 0.0001	3.00 ± 0.08	49.0 ± 2	3.6236 ± 0.0001	5.1516 ± 0.0002	6.90 ± 0.01
Lava™ Esthetic	4.84 / 0.113	23.7 ± 0.5	5.1340 ± 0.0001	4.6 ± 0.4	35.0 ± 3	3.6066 ± 0.0002	5.1779 ± 0.0001	2.78 ± 0.03	41.0 ± 2	3.6227 ± 0.0001	5.1527 ± 0.0001	6.70 ± 0.01
Cercon® xt	5.38 / 0.063	26.3 ± 0.2	5.1350 ± 0.0001	4.56 ± 0.04	22.3 ± 0.1	3.6093 ± 0.0001	5.1791 ± 0.0002	2.99 ± 0.03	51.4 ± 0.1	3.6237 ± 0.0001	5.1523 ± 0.0001	6.85 ± 0.01
Prettau® Anterior	5.40 / 0.063	26.0 ± 0.7	5.1351 ± 0.0003	5.0 ± 0.2	24.0 ± 1	3.6092 ± 0.0002	5.1779 ± 0.0006	3.07 ± 0.07	50.0 ± 2	3.6235 ± 0.0001	5.1535 ± 0.0001	6.73 ± 0.01

Table 5. Bulk Y_2O_3 / Al_2O_3 content (XRF), phase vol.% content (Rietveld), lattice parameters and Y_2O_3 content in each phase (determined from equations (1), (2) and (3)), according to a refinement considering the existence of only two tetragonal phases ($t + t''$). Values represent the means and standard deviations of two separate samples.

Material	Bulk mol% Y_2O_3 / Al_2O_3 (XRF)	t (Y-lean)				t'' (Y-rich)			
		vol.%	a [Å]	c [Å]	mol% Y_2O_3	vol.%	a [Å]	c [Å]	mol% Y_2O_3
IPS e.max® ZirCAD MO	3.08 / 0.300	69.1 ± 0.8	3.6044 ± 0.0001	5.1797 ± 0.00009	2.38 ± 0.005	30.9 ± 0.8	3.6219 ± 0.00028	5.1543 ± 0.00008	6.46 ± 0.027
Lava™ Plus	3.15 / 0.111	67.7 ± 0.1	3.6047 ± 0.00003	5.1791 ± 0.00011	2.46 ± 0.005	32.4 ± 0.1	3.6209 ± 0.00009	5.1553 ± 0.00024	6.26 ± 0.031
Cercon® ht	3.12 / 0.049	69.0 ± 0.5	3.6049 ± 0.00008	5.1795 ± 0.00005	2.45 ± 0.005	31.0 ± 0.5	3.6215 ± 0.00003	5.1565 ± 0.00018	6.24 ± 0.012
Prettau®	3.04 / 0.000	70.8 ± 0.1	3.6052 ± 0.00004	5.1798 ± 0.00009	2.47 ± 0.003	29.2 ± 0.1	3.6216 ± 0.00021	5.1518 ± 0.00009	6.12 ± 0.033
Katana™ ML	4.07 / 0.112	59.3 ± 0.7	3.6040 ± 0.00004	5.1806 ± 0.00021	2.27 ± 0.021	40.7 ± 0.7	3.6230 ± 0.00002	5.1495 ± 0.00026	7.00 ± 0.025
IPS e.max® ZirCAD MT	4.28 / 0.050	53.5 ± 0.7	3.6053 ± 0.00005	5.1802 ± 0.00011	2.44 ± 0.015	46.6 ± 0.7	3.6232 ± 0.00005	5.1519 ± 0.00001	6.81 ± 0.007
Katana™ STML	5.36 / 0.000	36.4 ± 4.2	3.6095 ± 0.00065	5.1793 ± 0.00090	2.99 ± 0.145	63.7 ± 4.2	3.6245 ± 0.00012	5.1496 ± 0.00023	7.16 ± 0.033
Lava™ Esthetic	4.84 / 0.113	41.2 ± 2.3	3.6059 ± 0.00005	5.1800 ± 0.00019	2.54 ± 0.020	58.8 ± 2.3	3.6234 ± 0.00003	5.1515 ± 0.00009	6.88 ± 0.011
Cercon® xt	5.38 / 0.063	33.1 ± 0.3	3.6095 ± 0.00012	5.1799 ± 0.00027	2.95 ± 0.035	66.9 ± 0.3	3.6245 ± 0.00004	5.1507 ± 0.00005	7.08 ± 0.001
Prettau® Anterior	5.40 / 0.063	37.1 ± 4.8	3.6095 ± 0.00046	5.1779 ± 0.00200	3.10 ± 0.209	62.9 ± 4.8	3.6241 ± 0.00019	5.1510 ± 0.00084	7.01 ± 0.048

Table 6. Bulk Y_2O_3 / Al_2O_3 content (XRF), phase vol.% content (Rietveld), lattice parameters and Y_2O_3 content in each phase for the material Innovnano 2YSZ at the surface of as-sintered samples, or after grinding (interior).

Material	Bulk mol% Y_2O_3 / Al_2O_3 (XRF)	$t - Y$ -lean				monoclinic			
		vol.%	a [Å]	c [Å]	mol% Y_2O_3	vol.%	a [Å]	b [Å]	c [Å]
Interior	1.89 / 0.429	82.8 ± 0.6	3.60240 ± 0.0002	5.17449 ± 0.00008	2.51 ± 0.03	17.2 ± 0.6	5.0855 ± 0.001	5.1581 ± 0.0011	5.3391 ± 0.0009
Surface		64.0 ± 2.0	3.60288 ± 0.00008	5.18190 ± 0.0001	2.006 ± 0.001	36 ± 2.0	5.1553 ± 0.0008	5.2005 ± 0.0008	5.3332 ± 0.0011

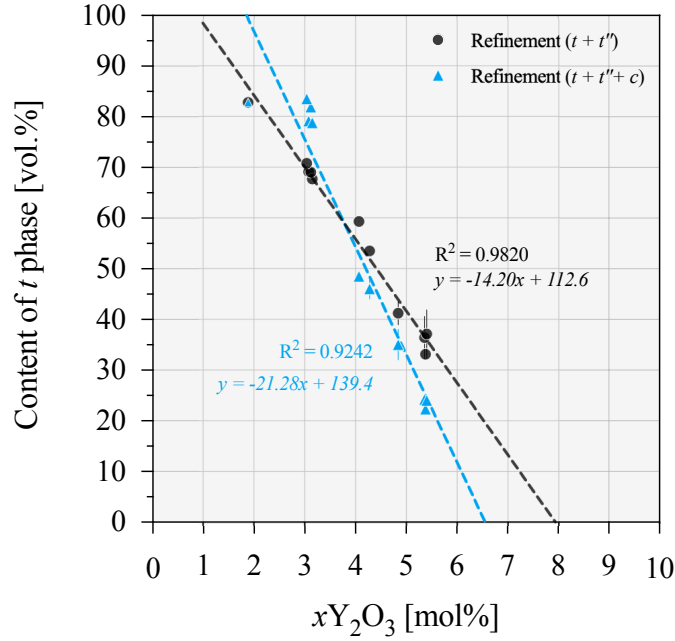


Fig. 6. Comparison of the relationships between t -phase content and bulk xY_2O_3 fraction for the two refinement approaches.

3.2.3. Fracture toughness

The measured values of Young's modulus, density, Poisson's ratio and fracture toughness for the sintered materials are summarized in Table 7. Within the margin of error, all materials yielded comparable values of ρ , E , and ν , with eventual exceptions, such as a density below 6.0 g/cm^3 for KatanaTM STML and IPS e.max[®] ZirCAD MO, and a relatively high Poisson's ratio of 0.350 ± 0.01 for KatanaTM ML.

Table 7. Elastic properties (E , ν), density (ρ) and fracture toughness (K_{Ic}) of the sintered samples. Different uppercase letters within a column represent statistical difference at $\alpha = 0.05$.

Material	E [GPa]	ν	ρ [g/cm ³]	K_{Ic} [MPa√m]
IPS e.max [®] ZirCAD MO	212.7 ± 1.1	0.315 ± 0.010	5.976 ± 0.039	4.90 ± 0.19 ^a
Lava TM Plus	214.3 ± 1.1	0.314 ± 0.010	6.053 ± 0.014	4.45 ± 0.26 ^{bc}
Cercon [®] ht	214.2 ± 1.1	0.317 ± 0.010	6.069 ± 0.017	4.87 ± 0.16 ^a
Prettau [®]	214.1 ± 1.1	0.313 ± 0.010	6.080 ± 0.016	4.57 ± 0.39 ^{abc}
Katana TM ML	217.4 ± 1.1	0.350 ± 0.010	6.041 ± 0.016	4.27 ± 0.25 ^c
IPS e.max [®] ZirCAD MT	215.7 ± 1.1	0.314 ± 0.010	6.035 ± 0.018	3.45 ± 0.24 ^d
Katana TM STML	214.5 ± 1.1	0.314 ± 0.010	5.988 ± 0.037	2.64 ± 0.14 ^g
Lava TM Esthetic	215.3 ± 1.1	0.314 ± 0.010	6.053 ± 0.018	3.26 ± 0.31 ^{dc}
Cercon [®] xt	216.2 ± 1.1	0.315 ± 0.010	6.0256 ± 0.008	2.80 ± 0.23 ^{fg}
Prettau [®] Anterior	216.9 ± 1.1	0.312 ± 0.010	6.016 ± 0.014	3.05 ± 0.13 ^{ef}
Innovnano 2YSZ	-	-	-	8.87 ± 0.18 ^g

In Fig. 7a our measured K_{Ic} -values are plotted relative to the mol% Y_2O_3 , and complemented by additional data from the literature for a wide range of mol% xY_2O_3 , in order to probe the spectrum of microstructural fraction from fully-monoclinic ($x = 0$) up to fully-cubic ($x = 8$). The literature values were selected so to contain only measurements from sharp-crack methods in order to avoid, particularly, single-edge-notched-beam results that are known to be subjected to a confounding notch-root radius effect [11, 12]. Despite being aware of the likewise questionable accuracy of Vickers-indentation-based methods for the testing of fracture toughness of coarse-grained ceramics [48-52], the shortage of studies employing other methodologies that would cover a wider range of Y_2O_3 stabilization left us with no other alternative. Those include classical studies such as that of Lange (1982) [53] and Masaki (1986) [54], both using Vickers indentation, which agree fairly well within $2.5 \leq x \leq 5.5$, but diverge for $1.5 \leq x < 2.5$. The work of Lange, despite seemingly overestimating the K_{Ic} for $x > 4.0$ and underestimating it for $x \leq 2.0$ – when based solely on the pooled values in Fig. 7 – still enjoys today a distinguished standing of establishing the relationship between K_{Ic} and xY_2O_3 (see for example Refs. [55, 56]).

The data in Fig. 7 was tentatively fitted to an exponential function of the form $K_{Ic}(xY_2O_3) = K_0 e^{-\lambda x} + K_{Ic,cubic}$. An exponential constant λ of $-1.102 \text{ mol}\%^{-1}$ is obtained by fitting to all the data for $x > 0$, and $\lambda = -0.888 \text{ mol}\%^{-1}$ by fitting only to the K_{Ic} -values obtained by the CNB method in this study. K_0 , which should theoretically represent the K_{Ic} -value of purely monoclinic zirconia, serves here merely as fitting parameter, since pure monoclinic zirconia is non-transformable and has been measured to have a K_{Ic} of $2.6 \text{ MPa}\sqrt{\text{m}}$ measured by Vickers [55, 57], up to $3.7 - 6.0 \text{ MPa}\sqrt{\text{m}}$ using a short-rod Chevron-notch specimen [58]. The curve fit to all the data obtains $K_{Ic,cubic} = 3.11 \text{ MPa}\sqrt{\text{m}}$, and $K_{Ic,cubic} = 2.70 \text{ MPa}\sqrt{\text{m}}$ if only fitted to our data, both substantially overestimating the experimentally obtained values by Cutler et al. [58], Liu et al. [59] and Cui et al. [60]. The poor goodness-of-fit seen for the fit to all the data results, on the one hand, due to the high variability in K_{Ic} -values among studies for $x > 3.0$, and the small number of data-points available for $x < 2.0$ on the other hand (e.g. [57]).

Considering that the increase in toughening in transformable YSZ, compared to non-transformable microstructures, is given by the tetragonal to monoclinic transformation (transformation toughening) [61], understanding the relationship between K_{Ic} and the amount of t -phase (Y-lean) becomes imperative. That relationship is attempted in Fig. 7b through a linear and a power-law fitting to our data, with the former excluding the 1.9 mol% Y_2O_3 material, and with the latter having the same form as in Fig. 7a, i.e. $K_{Ic}(xY_2O_3) = K_0 e^{\lambda x} + K_{cubic}$. The power-law gives a better fit than the linear regression, with comparable goodness-of-fit than the inverse power law between K_{Ic} and xY_2O_3 (Fig 7a), yet still overestimating $K_{Ic,cubic}$ ($2.86 \text{ MPa}\sqrt{\text{m}}$). If forced through the experimental $K_{Ic,cubic}$ value of $\sim 1.7 \text{ MPa}\sqrt{\text{m}}$, R^2 drops to ~ 0.91 . Fig. 7b also plots the content of t -phase if refined considering the presence of a cubic phase (in blue), and shows the inability to fit a proper power-law relationship. Because the behavior of K_{Ic} vs. xY_2O_3 and vs. t -phase vol.% departs from a mostly linear behavior at $x > 3.0$ (as also obtained in Ref. [62] using double-torsion specimens), to an exponential behavior taking place mostly between $2.0 \leq x \leq 3.0$, not only the amount but also the transformability of the t -phase, and supposedly other contributing factors, seem to play a role in the increase in K_{Ic} . Higher K_{Ic} -values with increasing t -phase content reflects the probabilistic nature of a crack encountering transformable grains in its path, responsible for toughening via the $t \rightarrow m$ mechanism. This relationship is not straightforward, since only a fraction of all t -grains is actually susceptible to transformation. To give an example, for the 1.9YSZ evaluated in Ref. [63] (green diamond in Fig. 7a) 77% of the $\sim 93 \text{ wt}\%$ t -phase transformed at fracture, while for a 3YSZ this amounted to only 2%. Basu et al. [64] reported a 57% t -phase transformability for a 2YSZ, 32% for a 2.5YSZ and 3% for a 3YSZ on fractured surfaces.

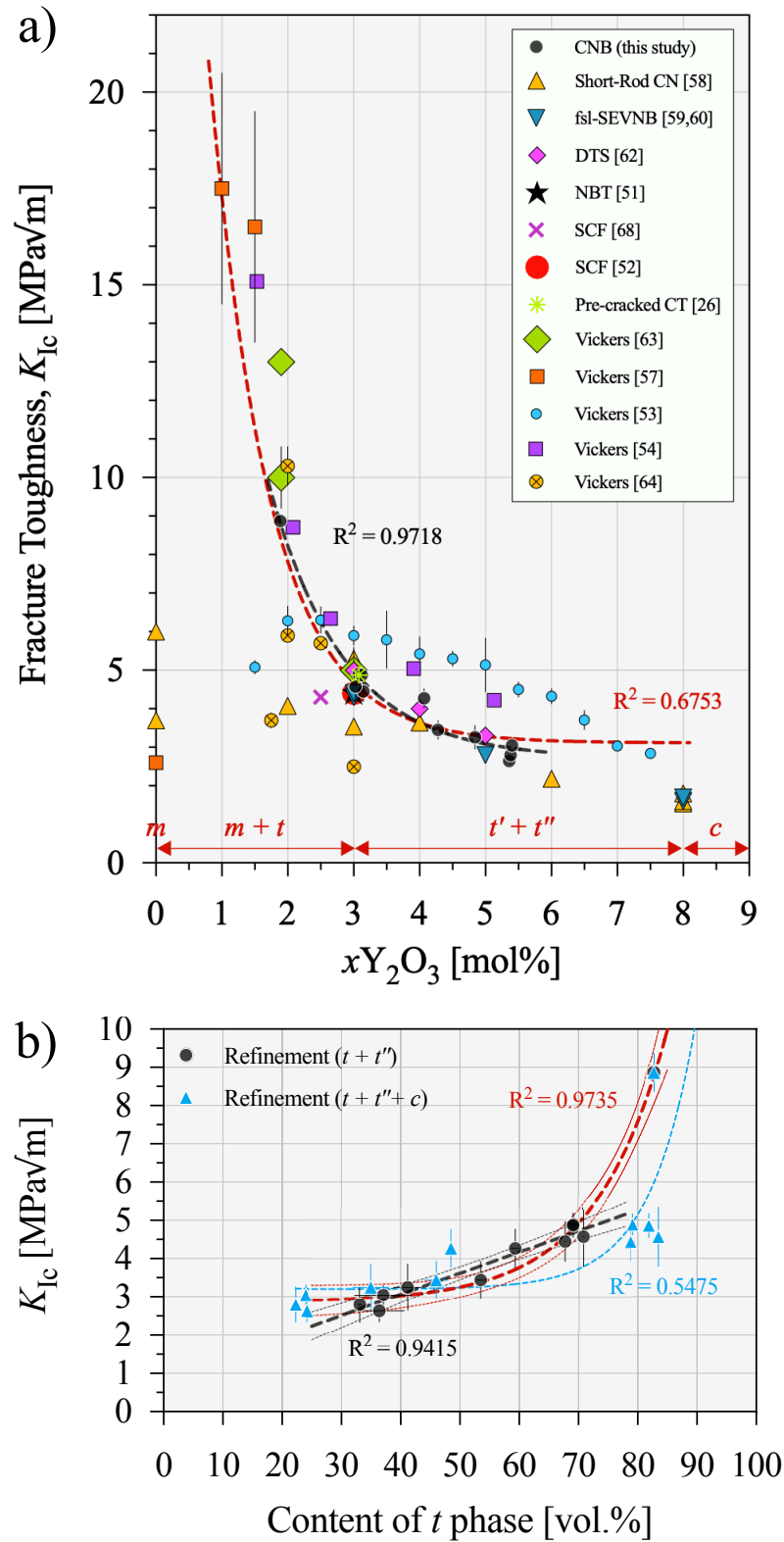


Fig. 7. (a) Attempted relationship between K_{Ic} and mol% Y_2O_3 content fitted to only our data-points (black dashed line) or to all data-points with $x > 0$ (red dashed line). (b) Attempted relationship between K_{Ic} and bulk content of t -phase [in vol.%] for the two refinement approaches; black dashed line is a linear regression excluding the Innovnano material. Dashed colored lines are power-law fits to all the data.

Interestingly, when mixing Tosoh grades TZ-3Y and TZ-0Y (pure monoclinic) to obtain a nominal 2YSZ, they reported an initial 2.7% *m*-phase fraction and a Vickers- K_{Ic} of 10.3 MPa \sqrt{m} , 2 times higher than a material sintered solely from a Tosoh grade TZ-2Y that showed a 40.3% initial *m*-phase content. This was accredited to the lower Y₂O₃ content distributed across the grains in the mixed powder, but most striking is the contribution of the presence of monoclinic phase *ab initio*, supposedly due to microcracking around the grains relieving K_I at the crack tip [65]. At 82.8 vol.% *t*-phase content of the Innovnano material after grinding, the susceptibility to transformation, gauged by the amount of Y₂O₃ in the lattice (see Table 6) – controlling the mismatch in the coefficient of thermal expansion [66, 67] – becomes comparable to or lower than some of the other materials tested here, making the amount of *t*-phase alone hardly responsible for the nearly 2-fold gain in K_{Ic} , when compared to the 3.1 mol% Y₂O₃ materials having ~70 vol.% *t*-phase. The appearance of a ~18 vol.% *m*-phase during cooling through the $T_0(t/m)$ line might therefore have increased the hydrostatic stress induced on the neighboring tetragonal grains to decrease the threshold for transformation. The effect of microcracking on toughening is considerable, but still estimated to be at least 3 times lower than that of the transformation [68].

It has to be considered though, that some of the 17.2 vol.% *m*-phase measured in the Innovnano material might have been triggered by a *t*→*m* transformation due to grinding, which would suggest a bulk composition of a slightly higher *t*-phase content, to some unknown degree. The high amount of monoclinic phase at the (unground) surface of samples point to the high susceptibility of the *t*-phase in Innovnano to transformation (containing 1.9 mol% Y₂O₃ at the sintering temperature). One might therefore be tempted to suspect the sawing of the notches in the fully-sintered Innovnano CNB specimens to have induced some *t*→*m* transformation at the notch surface, thereby increasing K_I for pop-in of the subcritical crack and consequently leading to artificially higher K_{Ic} -values. We showed however, that this is not the case [69]. Therein we subjected CNB specimens to increasing degrees of hydrothermal-induced *t*→*m* transformation (up to 90 vol% *m*-phase content and up 25 μ m-thick transformed surface layer), and obtained K_{Ic} -values identical to those of fully-tetragonal specimens (not aged). Even if the *m*-phase increases the pop-in K_I , the crack geometric factor still must be at its maximum at that stage, being unable to affect K_I at criticality (K_{Ic}) as the crack propagates into the bulk material. One should also keep in mind that the CNB method induces substantial subcritical crack extension (>600 μ m) before fracture, a relevant aspect when dealing with materials showing resistance curve (R-curve) behavior. 3YSZs, for instance, have been shown to have a flat [70] or a very shallow [71] R-curve. Although studies focused on detecting any R-curve behavior in zirconias stabilized with > 3 mol% Y₂O₃ are generally lacking, this is expected to be negligible. R-curve effects in < 3 mol% Y₂O₃ stabilized zirconias are considerable [72] due to the aforementioned factors; the CNB placing the obtained K_{Ic} -values near the plateau value $K_{I,max}$.

Admittedly, the relationships in Fig. 7a are only tentative, with the intentional aim of avoiding to dissociate different types of zirconia based on application. Of course, several aspects weigh in as far as fracture toughness is concerned, from fundamental methodological aspects affecting result reliability, to the variability in factors related to material processing among studies, such as powder composition and homogeneity, sintering pressure, temperature and time, as well as grain size distribution. Although most studies use experimental materials, most rely on the *x*Y₂O₃ certified by the powder supplier, and rarely verify the actual stabilizer content and redistribution during sintering, especially if powder mixtures are used. The latter strategy is known to be the usual route by dental manufacturers to achieve their target composition; the given *x*Y₂O₃ can vary slightly, as pointed out here. Still, we offer an alternative to the relationship established by Lange [53], in closer agreement to the trend seen by Misaki

[54], and expose the need for more systematic evaluation using more trustworthy methods. It seems, however, from the relationships obtained in Fig. 7, that a power-law relationship between fracture toughness and Ytria content prevails regardless of categorization, whether for technical or biomedical applications.

Conclusions

We can conclude from our findings that the fracture toughness of the white-bodies of dental zirconias are independent of the stabilizer concentration, and are in the range of $0.4 - 0.7 \text{ MPa}\sqrt{\text{m}}$, which might indicate a high susceptibility to machining damage. Considering the phase equilibrium diagram and electron diffraction evidences, the phase assignment and quantification demonstrated that the refinement with only $t + t''$ phases seem to be more appropriate for the 3-5 mol% Y_2O_3 dental compositions, compared to the refinement additionally including a cubic phase. The fracture toughness (K_{Ic}) of the dense dental zirconia materials decreases with respect to the Y_2O_3 content from $\sim 5 \text{ MPa}\sqrt{\text{m}}$ for 3YSZ to $\sim 3 \text{ MPa}\sqrt{\text{m}}$ for 5YSZ. The K_{Ic} -value decreases exponentially relative to the Y_2O_3 concentration within 1-8 mol% range, a relationship intricately connected to the t -phase fraction in the material.

Acknowledgements

All the materials tested in this study, apart from those from the company Zirkonzahn GmbH, were kindly donated by the manufacturers. The authors hold no conflicts of interest with any of these companies.

References

- [1] Y. Zhang, B.R. Lawn, Novel Zirconia Materials in Dentistry, *J. Dent. Res.* 97(2) (2018) 140-147.
- [2] J.R. Kelly, P. Benetti, P. Rungruangnunt, A. Della Bona, The slippery slope - Critical perspectives on in vitro research methodologies, *Dent. Mater.* 28(1) (2012) 41-51.
- [3] S.C. Bayne, Correlation of clinical performance with 'in vitro tests' of restorative dental materials that use polymer-based matrices, *Dent. Mater.* 28(1) (2012) 52-71.
- [4] G.D. Quinn, On edge chipping testing and some personal perspectives on the state of the art of mechanical testing, *Dent. Mater.* 31(1) (2015) 26-36.
- [5] M. Wendler, R. Belli, A. Petschelt, D. Mevec, W. Harrer, T. Lube, R. Danzer, U. Lohbauer, Chairside CAD/CAM materials. Part 2: Flexural strength testing, *Dent. Mater.* 33(1) (2017) 99-109.
- [6] R. Belli, M. Wendler, J.I. Zorzin, U. Lohbauer, Practical and theoretical considerations on the fracture toughness testing of dental restorative materials, *Dent. Mater.* 34(1) (2018) 97-119.
- [7] P.F. Cesar, A. Della Bona, S.S. Scherrer, M. Tholey, R. van Noort, A. Vichi, R. Kelly, U. Lohbauer, ADM guidance-Ceramics: Fracture toughness testing and method selection, *Dent. Mater.* 33(6) (2017) 575-584.
- [8] S.S. Scherrer, U. Lohbauer, A. Della Bona, A. Vichi, M.J. Tholey, J.R. Kelly, R. van Noort, P.F. Cesar, ADM guidance-Ceramics: guidance to the use of fractography in failure analysis of brittle materials, *Dent. Mater.* 33(6) (2017) 599-620.
- [9] S.S. Scherrer, M. Melzlzi, C. Crottaz, M. Gahlert, E. Romelli, L. Marger, S. Durual, E. Vittecoq, Translational research on clinically failed zirconia implants, *Dent. Mater.* 35(2) (2019) 368-388.
- [10] R. Belli, S.S. Scherrer, U. Lohbauer, Report on fractures of trilayered all-ceramic fixed dental prostheses, *Case Stud. Eng. Fail.* 7 (2016) 71-79.
- [11] R. Damani, R. Gstrein, R. Danzer, Critical notch-root radius effect in SENB-S fracture toughness testing, *J. Eur. Ceram. Soc.* 16(7) (1996) 695-702.
- [12] R.J. Damani, C. Schuster, R. Danzer, Polished notch modification of SENB-S fracture toughness testing, *J. Eur. Ceram. Soc.* 17(14) (1997) 1685-1689.
- [13] Y. Zhang, Making yttria-stabilized tetragonal zirconia translucent, *Dent. Mater.* 30(10) (2014) 1195-1203.
- [14] I.D. 6872:2015, Dentistry - Ceramic materials, (2015).
- [15] C. Jovalekic, M. Zdujic, D. Poleti, L. Karanovic, M. Mitric, Structural and electrical properties of the $2\text{Bi}(2)\text{O}(3)$ center dot $3\text{ZrO}(2)$ system, *J. Solid State Chem.* 181(6) (2008) 1321-1329.
- [16] D.N. Wang, Y.Q. Guo, K.M. Liang, K. Tao, Crystal structure of zirconia by Rietveld refinement, *Schience in China, Series A: Mathematics, Physics, Astronomy* 42 (1999) 80-86.

- [17] R.A. Miller, J.L. Smialek, R.G. Garlick, Phase stability in plasma-sprayed, partially stabilized zirconia-yttria, *Adv. Ceram.* 3 (1981) 241-253.
- [18] H.G. Scott, Phase Relationships in Zirconia-Yttria System, *J. Mater. Sci.* 10(9) (1975) 1527-1535.
- [19] H. Toraya, Effect of Y_{0.5} Dopant on Unit-Cell Parameters of ZrO₂ at Low Contents of Y_{0.5}, *J. Am. Ceram. Soc.* 72(4) (1989) 662-664.
- [20] R. Belli, M. Wendler, D. de Ligny, M.R. Cicconi, A. Petschelt, H. Peterlik, U. Lohbauer, Chairside CAD/CAM materials. Part 1: Measurement of elastic constants and microstructural characterization, *Dent. Mater.* 33(1) (2017) 84-98.
- [21] ASTM C1421, Standard test methods for determination of fracture toughness of advanced ceramics at ambient temperature, ASTM International, 2010.
- [22] ISO 24370, Fine ceramics (advanced ceramics, advanced technical ceramics) - Test method for fracture toughness of monolithic ceramics at room temperature by chevron-notched beam (CNB) method, International Organization for Standardization (2005).
- [23] EN 144253, Advanced technical ceramics - Test method for determination of fracture toughness of monolithic ceramics - Part 3: Chevron notched beam (CNB) method, European Committee for Standardization (2010).
- [24] C. Krautgasser, Z. Chlup, P. Supancic, R. Danzer, R. Berrnjo, Influence of subcritical crack growth on the determination of fracture toughness in brittle materials, *Journal of the European Ceramic Society* 36(5) (2016) 1307-1312.
- [25] R. Belli, M. Wendler, A. Petschelt, T. Lube, U. Lohbauer, Fracture toughness testing of biomedical ceramic-based materials using beams, plates and discs, *J. Eur. Ceram. Soc.* 38(16) (2018) 5533-5544.
- [26] P. Curran, M. Cattani-Lorente, H.W.A. Wiskott, S. Durual, S.S. Scherrer, Grinding damage assessment for CAD-CAM restorative materials, *Dent. Mater.* 33(3) (2017) 294-308.
- [27] R. Belli, U. Lohbauer, F. Goetz-Neunhoeffler, K. Hurler, Crack-healing during two-stage crystallization of lithium (di)silicate glass-ceramics, *Dent. Mater.* 35 (2019) 1130-1145.
- [28] P. Hrma, W.T. Han, A.R. Cooper, Thermal Healing of Cracks in Glass, *J. Non-Cryst. Solids* 102(1-3) (1988) 88-94.
- [29] I. Denry, How and when does fabrication damage adversely affect the clinical performance of ceramic restorations?, *Dent. Mater.* 29(1) (2013) 85-96.
- [30] P. Faust Gouveia, L.M. Schabbach, J.C.M. Souza, B. Henriques, J.A. Labrincha, F.S. Silva, M.C. Fredel, J. Mesquita-Guimarães, New perspectives for recycling dental zirconia waste resulting from CAD/CAM manufacturing process, *J. Clean Prod.* 152 (2017) 454-463.
- [31] M. Inokoshi, H. Shimizu, K. Nozaki, T. Takagaki, K. Yoshihara, N. Nagaoka, F. Zhang, J. Vleugels, B. Van Meerbeek, S. Minakuchi, Crystallographic and morphological analysis of sandblasted highly translucent dental zirconia, *Dent. Mater.* 34(3) (2018) 508-518.
- [32] E. Camposilvan, R. Leone, L. Gremillard, R. Sorrentino, F. Zarone, M. Ferrari, J. Chevalier, Aging resistance, mechanical properties and translucency of different yttria-stabilized zirconia ceramics for monolithic dental crown applications, *Dent. Mater.* 34(6) (2018) 879-890.
- [33] N. Kolakarnprasert, M.R. Kaizer, D.K. Kim, Y. Zhang, New multi-layered zirconias: Composition, microstructure and translucency, *Dent. Mater.* 35(5) (2019) 797-806.
- [34] F. Zhang, M. Inokoshi, M. Batuk, J. Hadermann, I. Naert, B. Van Meerbeek, J. Vleugels, Strength, toughness and aging stability of highly-translucent Y-TZP ceramics for dental restorations, *Dent. Mater.* 32(12) (2016) e327-e337.
- [35] O. Fabrichnaya, F. Aldinger, Assessment of thermodynamic parameters in the system ZrO₂-Y₂O₃-Al₂O₃, *Z. Metallkd.* 95(1) (2004) 27-39.
- [36] S. Lakiza, O. Fabrichnaya, M. Zinkevich, F. Aldinger, On the phase relations in the ZrO₂-YO_{1.5}-AlO_{1.5} system, *J. Alloy Compd.* 420(1-2) (2006) 237-245.
- [37] V. Lanteri, R. Chaim, A.H. Heuer, On the Microstructures Resulting from the Diffusionless Cubic-]Tetragonal Transformation in ZrO₂-Y₂O₃ Alloys, *J. Am. Ceram. Soc.* 69(10) (1986) C258-C261.
- [38] J.M. Cairney, N.R. Rebollo, M. Ruhle, C.G. Levi, Phase stability of thermal barrier oxides: A comparative study of Y and Yb additions, *Int. J. Mater. Res.* 98(12) (2007) 1177-1187.
- [39] A.H. Heuer, R. Chaim, V. Lanteri, The Displacive Cubic-]Tetragonal Transformation in ZrO₂ Alloys, *Acta Metall. Mater.* 35(3) (1987) 661-666.
- [40] A.V. Virkar, R.L.K. Matsumoto, Ferroelastic Domain Switching as a Toughening Mechanism in Tetragonal Zirconia, *J. Am. Ceram. Soc.* 69(10) (1986) C224-C226.
- [41] J.A. Krogstad, M. Lepple, Y. Gao, D.M. Lipkin, C.G. Levi, Effect of Yttria Content on the Zirconia Unit Cell Parameters, *J. Am. Ceram. Soc.* 94(12) (2011) 4548-4555.
- [42] J.A. Krogstad, S. Kramer, D.M. Lipkin, C.A. Johnson, D.R.G. Mitchell, J.M. Cairney, C.G. Levi, Phase Stability of t'-Zirconia-Based Thermal Barrier Coatings: Mechanistic Insights, *J. Am. Ceram. Soc.* 94 (2011) S168-S177.

- [43] M. Yashima, N. Ishizawa, M. Yoshimura, High temperature x-ray diffraction study on cubic-tetragonal phase transition in the ZrO_2 - $RO_{1.5}$ Systems (R: Rare Earths). pp. 125-35, In: Science and Technology of Zirconia, Edited by S.P.S. Badwal, M.J. Bannister, and R.H.J. Hannink. Technomic Publishing, Lancaster, (1993).
- [44] K. Matsui, H. Horikoshi, N. Ohmichi, M. Ohgai, H. Yoshida, Y. Ikuhara, Cubic-formation and grain-growth mechanisms in tetragonal zirconia polycrystal, *J. Am. Ceram. Soc.* 86(8) (2003) 1401-1408.
- [45] D.M. Lipkin, J.A. Krogstad, Y. Gao, C.A. Johnson, W.A. Nelson, C.G. Levi, Phase Evolution upon Aging of Air-Plasma Sprayed t'-Zirconia Coatings: ISynchrotron X-Ray Diffraction, *J. Am. Ceram. Soc.* 96(1) (2013) 290-298.
- [46] J.A. Krogstad, Y. Gao, J.M. Bai, J. Wang, D.M. Lipkin, C.G. Levi, In Situ Diffraction Study of the High-Temperature Decomposition of t'-Zirconia, *J. Am. Ceram. Soc.* 98(1) (2015) 247-254.
- [47] J.A. Krogstad, R.M. Leckie, S. Kramer, J.M. Cairney, D.M. Lipkin, C.A. Johnson, C.G. Levi, Phase Evolution upon Aging of Air Plasma Sprayed t'-Zirconia Coatings: II-Microstructure Evolution, *J. Am. Ceram. Soc.* 96(1) (2013) 299-307.
- [48] M.S. Kaliszewski, G. Behrens, A.H. Heuer, M.C. Shaw, D.B. Marshall, G.W. Dransmann, R.W. Steinbrech, A. Pajares, F. Guiberteau, F.L. Cumbreira, A. Dominguezrodriguez, Indentation Studies on Y_2O_3 -Stabilized ZrO_2 . I. Development of Indentation-Induced Cracks, *J. Am. Ceram. Soc.* 77(5) (1994) 1185-1193.
- [49] H. Miyazaki, Y. Yoshizawa, Correlation of the indentation fracture resistance measured using high-resolution optics and the fracture toughness obtained by the single edge-notched beam (SEPB) method for typical structural ceramics with various microstructures, *Ceram. Int.* 42(6) (2016) 7873-7876.
- [50] H. Miyazaki, Y. Yoshizawa, A reinvestigation of the validity of the indentation fracture (IF) method as applied to ceramics, *J. Eu. Ceram. Soc.* 37(15) (2017) 4437-4441.
- [51] S. Strobl, T. Lube, O. Schoppl, Toughness measurement on ball specimens. Part II: Experimental procedure and measurement uncertainties, *J. Eur. Ceram. Soc.* 34(7) (2014) 1881-1892.
- [52] G.D. Quinn, R.J. Gettings, J.J. Kübler, Fracture toughness of ceramics by the surface crack in flexure method: Results from the VAMASround robin, *Ceram. Eng. Sci. Proc.* 15 (1994) 846-855.
- [53] F.F. Lange, Transformation Toughening .3. Experimental-Observations in the ZrO_2 - Y_2O_3 System, *J. Mater. Sci.* 17(1) (1982) 240-246.
- [54] T. Masaki, Mechanical-Properties of Toughened ZrO_2 - Y_2O_3 Ceramics, *J. Am. Ceram. Soc.* 69(8) (1986) 638-640.
- [55] J. Chevalier, L. Gremillard, A.V. Virkar, D.R. Clarke, The Tetragonal-Monoclinic Transformation in Zirconia: Lessons Learned and Future Trends, *J. Am. Ceram. Soc.* 92(9) (2009) 1901-1920.
- [56] C. Mercer, J.R. Williams, D.R. Clarke, A.G. Evans, On a ferroelastic mechanism governing the toughness of metastable tetragonal-prime (t') yttria-stabilized zirconia, *Proc. R. Soc. A* 463(2081) (2007) 1393-1408.
- [57] A. Bravo-Leon, Y. Morikawa, M. Kawahara, M.J. Mayo, Fracture toughness of nanocrystalline tetragonal zirconia with low yttria content, *Acta Mater.* 50(18) (2002) 4555-4562.
- [58] R.A. Cutler, J.R. Reynolds, A. Jones, Sintering and Characterization of Polycrystalline Monoclinic, Tetragonal, and Cubic Zirconia, *J. Am. Ceram. Soc.* 75(8) (1992) 2173-2183.
- [59] H. Liu, W. Zhao, Y. Ji, J.P. Cui, Y.H. Chu, P.G. Rao, Determination of fracture toughness of zirconia ceramics with different yttria concentrations by SEVNB method, *Ceram. Inter.* 43(13) (2017) 10572-10575.
- [60] J.P. Cui, Z.Y. Gong, P.G. Rao, Effect of molten zone ablated by femtosecond laser on fracture toughness of oxide ceramics, *J. Eur. Ceram. Soc.* 38(5) (2018) 2440-2444.
- [61] M. Ruhle, A.G. Evans, High Toughness Ceramics and Ceramic Composites, *Prog. Mater. Sci. Prog. Mater. Sci.* 33(2) (1989) 85-167.
- [62] F. Zhang, H. Reveron, B.C. Spies, B. Van Meerbeek, J. Chevalier, Trade-off between fracture resistance and translucency of zirconia and lithium-disilicate glass ceramics for monolithic restorations, *Acta Biomater.* 91 (2019) 24-34.
- [63] A. Smirnov, H.D. Kurland, J. Grabow, F.A. Muller, J.F. Bartolome, Microstructure, mechanical properties and low temperature degradation resistance of 2Y-TZP ceramic materials derived from nanopowders prepared by laser vaporization, *J. Eur. Ceram. Soc.* 35(9) (2015) 2685-2691.
- [64] B. Basu, J. Vleugels, O. Van der Biest, Toughness tailoring of yttria-doped zirconia ceramics, *Mater. Sci. Eng. A* 380(1-2) (2004) 215-221.
- [65] M. Ruhle, N. Claussen, A.H. Heuer, Transformation and Microcrack Toughening as Complementary Processes in ZrO_2 -Toughened Al_2O_3 , *J. Am. Ceram. Soc.* 69(3) (1986) 195-197.
- [66] S. Schmauder, H. Schubert, Significance of Internal-Stresses for the Martensitic-Transformation in Yttria-Stabilized Tetragonal Zirconia Polycrystals during Degradation, *J. Am. Ceram. Soc.* 69(7) (1986) 534-540.
- [67] H. Schubert, Anisotropic Thermal-Expansion Coefficients of Y_2O_3 -Stabilized Tetragonal Zirconia, *J. Am. Ceram. Soc.* 69(3) (1986) 270-271.
- [68] D. Casellas, F.L. Cumbreira, F. Sanchez-Bajo, W. Forsling, L. Llanes, M. Anglada, On the transformation toughening of Y-ZrO₂ ceramics with mixed Y-TZP/PSZ microstructures, *J. Eur. Ceram. Soc.* 21(6) (2001) 765-777.

- [69] R. Belli, C. Loher, A. Petschelt, M.R. Cicconi, D. de Ligny, M. Anglada, U. Lohbauer, Low-temperature degradation increases the cyclic fatigue resistance of 3Y-TZP in bending, *Dent. Mater.* 36(8) (2020) 1086-1095.
- [70] R.H.J. Hannink, P.M. Kelly, B.C. Muddle, Transformation toughening in zirconia-containing ceramics, *J. Am. Ceram. Soc.* 83(3) (2000) 461-487.
- [71] J. Chevalier, P. Taddei, L. Gremillard, S. Deville, G. Fantozzi, J.F. Bartolome, C. Pecharroman, J.S. Moya, L.A. Diaz, R. Torrecillas, S. Affatato, Reliability assessment in advanced nanocomposite materials for orthopaedic applications, *J. Mech. Behav. Biomed. Mater.* 4(3) (2011) 303-314.
- [72] D. Casellas, J. Alcala, L. Llanes, M. Anglada, Fracture variability and R-curve behavior in yttria-stabilized zirconia ceramics, *J. Mater. Sci.* 36(12) (2001) 3011-3025.